


RESEARCH

Open Access



Sema4D deficiency enhances glucose tolerance through GLUT2 retention in hepatocytes

Yanling Zhang^{1†}, Xiaomei Jiang^{1†}, Dongsong Wu¹, Hao Huang¹, Guiqing Jia¹ and Gaoping Zhao^{1,2*} 

Abstract

Background The glucose transporter 2 (GLUT2) is constitutively expressed in pancreatic beta cells and hepatocytes of mice. It is the most important receptor in glucose-stimulated insulin release and hepatic glucose transport. The Sema4D is a signalin receptor on cell membranes. The correlation between Sema4D and GLUT2 has not been reported previously. We investigated whether knockdown of Sema4D could exert a hypoglycemic effect based on the increased GLUT2 expression in Sema4D ^{-/-} mice hepatocytes.

Methods The glucose tolerance test and insulin tolerance test in sema4D ^{-/-} and sema4D ^{+/+} mice were compared before and after streptozotocin (STZ) injection; the expression of GLUT2 content on the membrane surface of both groups was verified by Western blot. Then, the levels of insulin and C-peptide in the serum of the two groups of mice after STZ injection were measured by ELISA; the differentially expressed mRNAs in the liver of the two groups of mice were analyzed by transcriptomic analysis; then the differences in the expression of GLUT2, glycogen, insulin and glucagon in the two groups of mice were compared by tissue section staining. Finally, metabolomics analysis was performed to analyze the metabolites differentially expressed in the two groups of mice.

Key findings First, Sema4D ^{-/-} male mice exhibited significantly greater glucose tolerance than wild-type mice in a hyperglycemic environment. Secondly, Sema4D ^{-/-} mice had more retained GLUT2 in liver membranes after STZ injection according to an immunofluorescence assay. After STZ injection, Sema4D ^{-/-} male mice did not exhibit fasting hyperinsulinemia like wild-type mice. Finally, analysis of metabolomic and immunohistochemical data also revealed that Sema4D ^{-/-} mice produce hypoglycemic effects by enhancing the pentose phosphate pathway, but not glycogen synthesis.

Conclusions Thus, Sema4D may play an important role in the regulation of glucose homeostasis by affecting GLUT2 synthesis.

Keywords Sema4D/CD100, GLUT2, Insulin resistance, Streptozotocin, Glucose tolerance

[†]Yanling Zhang and Xiaomei Jiang made an equal contribution to this study.

*Correspondence:

Gaoping Zhao
gzhao@uestc.edu.cn

¹Department of Gastrointestinal Surgery, Sichuan Academy of Medical Sciences and Sichuan Provincial People's Hospital, University of Electronic

Science and Technology of China, 32 West Second Section, First Ring Road, Chengdu 610072, China

²Clinical Immunology Translational Medicine Key Laboratory of Sichuan Province, Sichuan Academy of Medical Sciences and Sichuan Provincial People's Hospital, University of Electronic Science and Technology of China, Chengdu 610072, China



© The Author(s) 2024. **Open Access** This article is licensed under a Creative Commons Attribution-NonCommercial-NoDerivatives 4.0 International License, which permits any non-commercial use, sharing, distribution and reproduction in any medium or format, as long as you give appropriate credit to the original author(s) and the source, provide a link to the Creative Commons licence, and indicate if you modified the licensed material. You do not have permission under this licence to share adapted material derived from this article or parts of it. The images or other third party material in this article are included in the article's Creative Commons licence, unless indicated otherwise in a credit line to the material. If material is not included in the article's Creative Commons licence and your intended use is not permitted by statutory regulation or exceeds the permitted use, you will need to obtain permission directly from the copyright holder. To view a copy of this licence, visit <http://creativecommons.org/licenses/by-nc-nd/4.0/>.

Introduction

Type 2 diabetes mellitus (T2D) is a global chronic metabolic disease characterized by persistent elevation of blood glucose. As of 2017, there were 425 million people with diabetes worldwide, 90% of whom had T2D and by 2045 this number is estimated to reach 629 million [1]. As a result a large number of treatment options for diabetes have been introduced, such as pharmacotherapy, insulin, and insulin analogs, surgical and nutritional therapy, diet management and exercise for weight loss [2]. However, the treatment of diabetes remains very complex and long and comprehensive and new therapeutic modalities and drugs are still being discovered.

The GLUT2 transmembrane carrier protein is the major glucose transporter isoform in pancreatic β -cells, liver, kidney, and small intestine, and regulates the sensitivity of pancreatic β -cells and hepatocytes to glucose [3]. It has been shown that increased GLUT2 expression in rat pancreatic β -cells increases hepatic glycogen synthesis thereby reducing blood glucose levels [4]. By increasing the expression of GLUT2 in pancreatic β -cells of DB/DB mouse, insulin resistance was shown to be improved resulting in lower blood glucose levels [5]. Pancreatic β -cells sense blood glucose concentration through GLUT2 and thus regulate glucose homeostasis [6]. Metabolites of some drugs can increase GLUT2 expression in insulin-resistant hepatocytes and inhibit gluconeogenesis, thereby lowering blood glucose [7]. Mice lacking GLUT2 expression do not survive into adulthood, while mutations in the glucose transporter protein 2 gene (GLUT2) in young children, known as the Fanconi-Bickel syndrome, is characterized by a reversible hyperglycemic state in infancy and the accumulation of renal glycogen [8]. Mutations in the SLC2A2 gene that encodes GLUT2 are associated with the transition from impaired glucose tolerance to T2D and increase the risk of developing diabetes [9]. Polymorphisms in SLC2A2 encode the glucose transporter GLUT2 and are important determinants of the response to metformin [10]. All the above evidence emphasizes the important role of GLUT2 in the regulation of glucose metabolism homeostasis.

Semaphorin 4D or Cluster of Differentiation 100 (Sema4D/CD100) is a homodimeric protein that belongs to the signaling protein family of axon guidance proteins. Members of this signaling protein family have received increasing attention in recent years due to their multiple functions in the immune system. Sema4D was the first signaling protein described to have an immune function and plays an important role in T cell initiation, antibody production, and intercellular adhesion. Sema4D is induced by hypoxia in a HIF-1-dependent manner and acts on endothelial cells via clumping protein B1, which has been shown to promote angiogenesis and enhance aggressive growth and proliferation in certain tumors

[11]. Sema4D also accelerates wound healing in diabetic mice by promoting wound angiogenesis and reducing the inflammatory response [12]. In turn, inhibition of the Sema4D/PlexinB1 signaling pathway attenuates vascular dysfunction in diabetic retinopathy [13]. However, no relationship between Sema4D and glucose regulation has been reported and we showed accidentally during a study to establish a Sema4D $-/-$ mice model of diabetes using mice islet transplantation and STZ that these mice had increased GLUT2 expression in hepatocytes and pancreatic β -cells compared to that observed in wild-type mice. Based on this phenomenon, we investigated the effect of knockdown of Sema4D on blood glucose regulation.

Materials and methods

Animals

Sema4D $-/-$ mice were purchased from Cyagen (Suzhou, China), while the Sema4D knockout mice model (C57BL/6) was created by CRISPR/Cas9-mediated genome engineering. The Sema4D gene (NCBI reference sequence: NM_013660; Ensembl: ENSMUSG00000021451) is located on mice chromosome 13. Sixteen exons have been identified, with the ATG start codon in exon 3 and the TGA stop codon in exon 16 (transcript, ENSMUST00000021900). Exons 5~7 were selected as the target sites. cas9 and gRNA were co-injected into fertilized eggs for production of the KO mice model. The pups were genotyped by PCR and sequencing analysis. Exon 5 starts at approximately 9.79% of the coding region, while exons 5 to 7 account for 9.91% of the coding region. The size of the effective KO region was ~7587 bp. The KO region does not have any other known genes. The C57BL/6 mice were purchased from Chengdu Pharmacies Biotechnology Co (Chengdu, China). After breeding Sema4D knockout mice and wild-type mice for approximately one year, age-matched mice were selected for experimentation. The diabetes model was constructed by intraperitoneal injection of 100 mg/kg of STZ in mice after 8–12 h of fasting. Mice were housed in a specific pathogen free facility and were provided with adequate water and food. All procedures were approved by the Animal Care and Use Committee of the Animal Research Institute of the Sichuan Provincial People's Hospital on March 1, 2017 under the ethical number 65 of 2017 Ethics (Research).

Genotype identification

A 100 μ L aliquot of digestion buffer (10503027, Invitrogen, Californian, USA) per toe (2–5 mm) was added to a microcentrifuge tube, being careful not to cut too many toes. The tubes were incubated at 56 °C overnight, followed by incubation with proteinase K at 98 °C for 13 min to denature the protein. The tube was then spun at maximum speed for 15 min in a microcentrifuge. PCR

was performed using a small amount of supernatant (1 μ L, 12.5 μ L reaction) taken directly from the tubes. The final concentration of the toe digestion buffer was 50 mM KCl, 10 mM Tris-HCl (pH 9.0), 0.1% TritonX-100, and 0.4 mg/mL proteinase K.

The reaction system contained 1 μ L of upstream and downstream primers, 20.5 μ L of Gold MIX enzyme, and 2.5 μ L of DNA. The amplification conditions were set according to the Gold MIX enzyme product instructions, with the amplification products finally electrophoresed in 1-3% agarose gel and analyzed to determine the genotype (Fig. S1).

PCR Screening.

Primers 1: (Annealing temperature 60.0°C)

F1: 5'-CTGTTCTTGGCCCTGGTGGTAGTG-3'

R1: 5'-TAGAAGTGAGACCTACCGTGAAAGCG-3'

Product size: 538 bp.

Primers 2: (Annealing temperature 60.0°C)

F3: 5'-GTCACAGAGTCAGGGACCTTGGGAAG-3'

R3: 5'-CTCATGGGTGTCTCTCCAGGTGG-3'

Product size: 352 bp.

Homozygotes: one band with 538 bp.

Heterozygotes: three bands with 538 bp and 352 bp.

Wildtype allele: two bands with 352 bp.

Enzyme-linked immunosorbent assay (ELISA)

The mice insulin (INS) kit and mice C-peptide (C-P) kit (Ruixinbio, Quanzhou, China) were used to perform double antibody sandwich enzyme-linked immunosorbent assays. After warming and sufficient washing, the unbound components were removed and a solid phase antibody-antigen-enzymatic antibody sandwich complex formed on the solid phase surface of the microtiter plate. Substrates A (0.01% hydrogen peroxide) and B (0.1% TMB) were added and the substrate catalyzed by HRP to produce a blue product, which was finally converted to yellow in the presence of the terminating solution (2 M sulfuric acid). The absorbance (OD) was measured at 450 nm wavelength using an enzyme marker (Rayto, RT-6100). The OD correlated positively with the concentration of the detectors in the samples to be tested. The concentration of the standard was used as the horizontal coordinate (6 standard wells, plus 1 0-value well, totaling 7 concentration points), and the corresponding OD value used as the vertical coordinate. Using computer software, a four-parameter logistic curve fit (4-pl) was used to create a standard curve that allowed the concentration value of the sample to be calculated from its OD. The calibration product dose response curve correlation coefficient, r value, was ≥ 0.9900 . The mice INS kit was calibrated at 40, 20, 10, 5, 2.5, and 1.25 mIU/L. The calibrator concentrations of the mice C-P kit were 12, 6, 3, 1.5, 0.75, and 0.375 ng/mL.

Immunoblotting

The harvested mice liver tissues were lysed with 200 μ L of P0013B RIPA strong lysis buffer (Beyotime, Shanghai, China) and PMSF then added within minutes to make a final concentration of 1 mM PMSF, followed by homogenization using a glass homogenizer (YJQ0928Q) Q. After sufficient lysis, the tissues were centrifuged at 10,000–14,000 g for 3–4 min and the supernatant removed for the BCA protein concentration assay. The protein concentration in the cell lysate was determined using the BCA protein assay kit (Therm Scientific, Californian, USA). A 1/4 volume of 5* SDS-PAGE protein loading buffer (P1040 Solarbio) was added to the protein samples followed by incubation in a metal bath at 100 °C for 10 min.

The prepared protein samples were then separated on SDS-PAGE gels and transferred to PVDF membranes. The PVDF membranes with the target proteins were closed with protein-free fast closing solution (Yarase, Shanghai, China) for 15–20 min followed by incubation overnight at 4 °C in 5% BSA containing glucose transporter GLUT2 antibody (C-10) (sc-518022 SantaCruz) or GAPDH mice mAb (HRP conjugate ZENBIO)/anti-CD100 (C-3) HRP (SC-390675HRP, SantaCruz, Californian, USA) and further incubation for 1 h at room temperature. The overnight incubated primary antibody was washed five times with TBST and then incubated with horseradish peroxidase-conjugated secondary antibody for 2 h at room temperature. After washing the antibody-incubated PVDF membrane three times with TBST (BL608A, Biosharp, Guangzhou, China), the membrane was incubated in a dark chamber with ECL luminescent solution (Millipore) for 1–3 min, and the protein bands visualized with the Invitrogen ibright intelligent imaging system (GoldBand 3-color regular range protein marker (10–180 kDa) (20351ES76, YEASEN, Shanghai, China).

Real time RT-PCR

The total RNA was extracted from mice liver tissue with TRIzol reagent (Invitrogen, Californian, USA) according to standard procedures. 1 μ g of total RNA was used for the reverse transcription reaction, while the SYBR green pro taq HS premix qPCR Kit (AG11701 Accurate Biology, Changsha, China) and the Evo M-MIV reverse transcription premix kit (AG11728 Accurate Biology, China) was used for the real-time qPCR assays. The mRNA expression levels were detected by the CFX Manager system (BioRad, Californian, USA).

GLUT2-F ACCGGGATGATGGCATGTT.

GLUT2-R GGACCTGGCCCAATCTCAAA.

Sema4D-F ACTACTCGGCCTTGCTGATG.

Sema4D-R AGGCATTCCTGCTTTGA.

MUP1-F GGGGAAACCTTCCAGCTGAT.

MUP1-R GCAGCGATGGCATTGGATAG.

MUP8-F ACCCTAGTGTGTGTCATGC.
MUP8-R AAGGAATTCTCCAAGACACGGA.
MUP9-F TCCAAGACATGGATTTGCTCCA.
MUP9-R GTAAGAGATGAAGAGTGCTCCGA.
MUP12-F TGGGACTGACCCTAGTGTGT.
MUP12-R TCCAAGACATGGATTTGCTCCA.
GAPDH-F ATGATTCCACCCATGGCAAATTC.
GAPDH-R GACTCCACGACGTACTCAGC.

HE and PAS staining

After euthanizing the donor mice, liver and pancreatic tissues were collected and fixed in 4% paraformaldehyde. Following dehydration using an automated dehydration machine, the tissues were embedded in paraffin for subsequent sectioning and analysis.

HE stains: hematoxylin staining for 10–20 min; tap water rinse for 1–3 min; hydrochloric acid alcohol fractionation for 5–10 s; tap water rinse for 1–3 min; placed into warm water at 50 °C or weak alkaline aqueous solution until a blue color appeared; tap water rinse for 1–3 min; and placed into 85% alcohol for 3–5 min. Eosin staining 3–5 min; water washing 3–5 s; gradient alcohol dehydration; xylene transparent; neutral gum sealing.

PAS stains: Tissue section were placed into periodate solution, oxidation for 5 min; placed into Schiff's reagent and dip staining for 10–20 min; Schiff's reagent poured off, rinsed with running water for 10 min; placed into hematoxylin staining solution for 1–2 min to stain nuclei; differentiated with hydrochloric acid differentiation solution for 2–5 s; washed with water; returned to blue with Scott's blueing solution; washed with water for 3 min; grade by grade conventional ethanol dehydration, xylene transparent, and neutral gum sealing. The specimens were then subjected to pathological examination using standard operating procedures (SOP) that included dehydration, trimming, embedding, sectioning, staining, sealing, and finally microscopic examination.

HE staining was performed using a Panoramic 250 digital section scanner manufactured by 3DHISTECH (Budapest, Hungary) to acquire images of the sections, with each section first examined at 40x to observe the general lesions, followed by acquisition of 100x and 400x images to observe the specific lesions. The positive expression area (area) within the acquired images was determined using the Image-Pro Plus 6.0 image analysis system (Media Cybernetics, Californian, USA), with the percentage positive expression area calculated as: positive expression area/area of view (pixel area). SPSS23.0 statistical analysis software was used to perform independent-sample t-tests on the data, with the data expressed as mean \pm standard deviation (mean \pm SD).

Immunofluorescence

Immunofluorescence analysis was performed to evaluate the expression of GLUT2 in mouse liver tissues and insulin and glucagon in pancreatic tissues. The tissue samples were fixed and embedded in paraffin for the following procedures. The paraffin sections were dewaxed to water; antigen repaired; dropwise addition of goat serum blocking solution; blocked at room temperature for 20 min; dropwise addition of glucose transporter GLUT2 antibody (C-10) (sc-518022 Santa Cruz, Californian, USA); incubation overnight at 4 °C; washed 3 times for 5 min each in PBS; dropwise addition of secondary antibody (CY3-labeled goat anti-mice) (GB21301 Servicebio, Wuhan, China) and incubation for 30 min at 37 °C; washed 3 times for 5 min each in PBS; dropwise addition of DAPI and incubation at room temperature for 10 min; washed 3 times for 5 min each in PBS; and sealing of the slices using anti-fluorescence attenuating sealer. Each section was first observed at 100 \times and then 100 \times and 400 \times microscopic images were acquired for a total of 3 fields of view. The integrated density (IntDen) and area (area) of all the acquired images were measured using the Image-J image analysis system and the mean gray value (mean) of each image then calculated. The mean fluorescence intensity of each sample was calculated using the mean fluorescence intensity of the two images. Similarly, insulin and glucagon expression were detected using insulin antibody (ab181547 abcam), secondary antibody (FITC-labeled goat anti-rabbit) (GB22303 Servicebio, Wuhan, China), glucagon antibody (ab10988 abcam), and secondary antibody (CY3-labeled goat anti-mice) (GB21301 Servicebio).

The DAPI-stained cell nuclei were blue, GLUT2 positive expression was red, insulin expression was green, and glucagon expression was red.

Glucose tolerance test and insulin tolerance test (GTT and ITT)

Fasting blood glucose levels were measured in 7–8week-old large *Sema4D* $-/-$ mice and *Sema4D* $+/+$ mice using a Roche blood glucose meter (ACCU-CHEK active blood glucose meter). The baseline blood samples were collected from the tail tip of the mice after they had fasted for 8–12 h without food, followed by intraperitoneal injection of 1 g/kg of glucose solution (A2494001. Gibco, Californian, USA). The blood glucose levels were measured 30, 60, and 120 min after the injection using the same method described above.

Fasting blood glucose levels were measured in 7–8week-old *Sema4D* $-/-$ mice and *Sema4D* $+/+$ mice after 4–6 h of fasting without food using a Roche blood glucose meter (ACCU-CHEK active blood glucose meter). A 0.5 μ g/kg aliquot of fast-acting insulin (Novo Nordisk, Copenhagen, Denmark) was injected intraperitoneally

and the blood glucose levels measured at 30, 60, and 120 min after the injection using the same method as described above.

Biochemical testing

Aliquots of mice serum were introduced into an automatic biochemical instrument (Hitachi 7180, Tokyo, Japan) to measure serum albumin levels using the ketoamine oxidase method. The detection principle of this assay was as follows: First, protease was used to degrade albumin in the serum into amino acid fragments. Ketoamine oxidase was then used to selectively oxidize fructose amino acids to generate hydrogen peroxide. Finally, the content of hydrogen peroxide was determined by Trinder's reaction, and the content of glycosylated albumin in the sample calculated.

Sequencing of mRNA

Transcriptome sequencing and basic analysis were provided by Shanghai Whale Gene Technology Co. Total RNA was extracted from the samples using the Tianmo #TR205-200 kit (Santa Clara, CA, US), according to the standard operating procedure manual provided by the manufacturer. The integrity of the RNA was tested and checked for total RNA concentration and purity using a Qubit[®] 3.0 fluorometer (Life Technologies, CA, USA), while a Nanodrop One spectrophotometer (Thermo Fisher Scientific Inc, Californian, USA) was used to check the concentration and purity of total RNA. Cluster generation and hybridization of the first-order sequencing primers were performed on the Illumina NovaSeq 6000 sequencer cBot according to the standard procedures in the cBot user's guide. The sequencing process was fully controlled by Illumina's data acquisition software, with the sequencing results analyzed in real time.

The sequencing raw data were saved as fastq format files (fq files), and after analysis and processing, the results were organized into expression values at the transcriptional level. The raw image data files obtained from high-throughput sequencing were converted to raw sequenced sequences by CASAVA base identification, with these sequence files referred to as raw reads. The main purpose of filtering sequences using fastp software was to exclude the following sequences.

1. Removal of primer splice sequences contained in the reads.
2. Removal of bases with a quality Q value < 20 at the 3' end of the reads.
3. Removal of reads with a sequence length < 25.
4. Removal of ribosomal RNA reads of the sequencing target species.

Hisat2 software was used for sequence alignment. Differential analysis of gene expression between samples/groups was performed using the edgeR software package. The *p*-value was calculated and then the multiple hypothesis test was corrected by controlling the FDR (false discovery rate) to determine the *p*-value threshold, with the corrected *p*-value called the Q-value. Meanwhile, the differential expression ploidy, or ploidy change, or FC, was calculated on the basis of the FPKM value, which is usually expressed as log₂(FC). Immediately after gene matching, the genes were annotated against the Gene Ontology (GO) and KEGG databases to determine gene-related functions and the pathways involved.

Metabolomics

In this study, mouse liver samples were selected for metabolomic analysis. After euthanizing the donor mice from both groups, a portion of the liver was rapidly placed in liquid nitrogen to quench metabolic-related enzymes. The tissue was subsequently stored at -80 °C for further analysis. Technical services were provided by Suzhou Panomic Biomedical Technology Co. A Thermo Vanquish (Thermo Fisher Scientific, USA) UPLC system was used with an ACQUITY UPLC[®] HSS T3 column (2.1 × 150 mm, 1.8 μm; Waters, Milford, MA, USA) with a flow rate of 0.25 mL/min and a column temperature of 40°C. The data were collected in the positive and negative ion mode using a Thermo Orbitrap Exploris 120 mass spectrometer (Thermo Fisher Scientific, USA) with an electrospray ionization source (ESI). The raw mass spectrometry downstream files were converted to the mzXML file format using the MSConvert tool in the Proteowizard package (v3.0.8789). Peak detection, filtering, and alignment were performed using the R XCMS package to obtain the list of substances for quantification, with the parameters set to bw=2, ppm=15, peak width=c (5, 30), mzwid=0.015, mzdiff=0.01, and method="centWave". The public databases HMDB, massbank, LipidMaps, mzcloud, KEGG and self-built substance libraries were used for substance identification with parameters set to < 30 ppm. Substances with a RSD > 30% in the QC samples were filtered out from the data quality control [14].

In this experiment, QC samples were used for quality control during the LC-MS assay. Orthogonal partial least squares discriminant analysis (OPLS-DA) was performed on the sample data using the R package Ropls to reduce dimensionality. The overfitting test of the model was performed using the envelope test. Metabolite molecules were considered statistically significant when their *P* values were < 0.05 and VIP values > 1. Functional pathway enrichment and topological analysis of the screened differential metabolite molecules were performed using the MetaboAnalyst software package. The enriched pathways

were browsed for differential metabolites and pathway maps using the KEGG Mapper visualization tool.

Statistical analysis

SPSS23.0 statistical analysis software was used to perform independent-sample T tests on the data, with the data expressed as mean \pm standard deviation (mean \pm SD). To verify the assumption of normal distribution, a homogeneity of variance test was conducted. The results indicated that the variances of the two groups were unequal. Consequently, a one-way ANOVA was utilized to compare the differences between the two groups. Two independent samples t-test and the Kolmogorov-Smirnov test were used to verify whether the data had a normal distribution. Two-way ANOVA in the Prism 9 Program (Graph Pad, San Diego, CA, USA) was used for the statistical analysis. p -values < 0.05 were considered to signify a statistically significant difference.

Results

Knockout of Sema4D increases expression of GLUT2 protein in liver tissue

A Sema4D $-/-$ mice model (Fig. 1A) was established by crisper cas9 technology, with a total of three knocked-out exons. Protein immunoblotting showed a significant

increase in hepatic GLUT2 protein in the knockout mice (Fig. 1B), which still had some amount of Sema4D translation. This may be because the knocked out exons are not sufficient to completely remove the translational expression of Sema4D protein. The expression of Sema4D visible in the knockout mice was due to part of the antigen being bound by the antibody used, which was not in the amino acid sequence translated by the three knocked out exons. Therefore, some of the post-transcription translated protein remained bound, although there was significantly reduced expression. Sema4D mRNA expression was reduced significantly in the Sema4D $-/-$ mice (Fig. 1C), with this difference being statistically significant. However, GLUT2 mRNA expression in the Sema4D $-/-$ mice was upregulated (Fig. 1D), although this difference was not statistically significant. This may be due to cascade amplification effects or epigenetic modifications in the transcription-to-translation process of the gene, which enhances the translation of GLUT2 mRNA. This suggests that the expression of GLUT2 protein may be increased during post-transcriptional translation. The expression of hepatic GLUT2 protein was verified by immunofluorescence, with hepatic GLUT2 expression being higher in the Sema4D $-/-$ mice (Fig. 1E), a finding consistent with the results of protein immunoblotting.

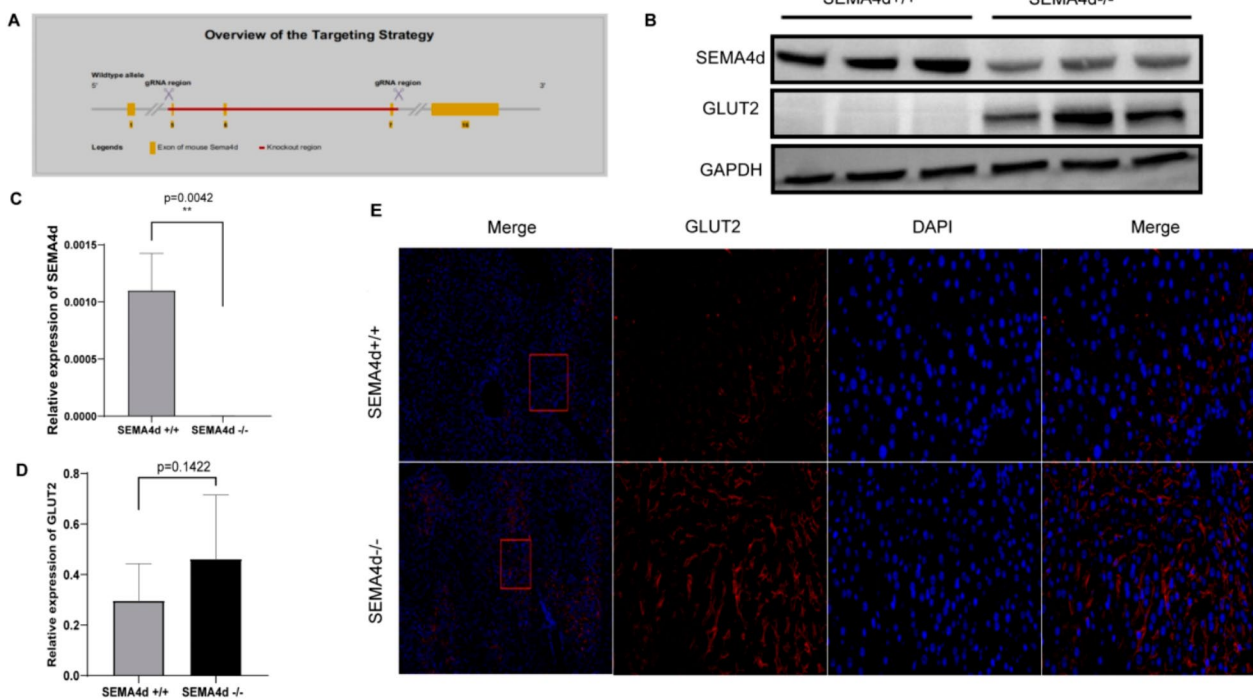


Fig. 1 Increased GLUT2 expression in Sema4D knockout mice. Schematic diagram of the Sema4D $-/-$ mice model established by CRISPR/cas9 technology (A). WB validation of the expression of Sema4D protein and GLUT2 protein in Sema4D $-/-$ mice versus Sema4D+/+ mice liver cells with GAPDH as an internal reference, $n = 3$ (B). RT-PCR validation of Sema4D mRNA (C) and GLUT2 mRNA (D) expression in liver tissues. The results are expressed as mean \pm SD. Immunofluorescence comparison of GLUT2 expression on liver cell membranes in Sema4D $-/-$ male mice versus Sema4D+/+ male mice (E). $n = 3$. The red box indicates the area magnified to 40x. The DAPI-stained nuclei are blue, while GLUT2 positive expression is red. The magnifications are 10x and 40x. * $p < 0.05$, ** $p < 0.01$

However, due to the small sample size, the data does not have statistical significance (the data is not shown).

Sema4D $-/-$ mice have increased insulin secretion through increased GLUT2

It has been demonstrated previously that GLUT2 is expressed specifically on mice liver and pancreatic β -cell membranes. We likewise observed increased GLUT2 expression in Sema4D $-/-$ mice liver with an immunofluorescence technique. In addition we observed that Sema4D $-/-$ mice expressed more pancreatic GLUT2 than that of wild-type mice (Fig. 2A), seen as increased fluorescence intensity (Fig. 2B). GLUT2 is the most important glucose sensing receptor and glucose transporter protein in mice pancreatic β -cells. We therefore measured serum insulin levels in male Sema4D $-/-$ mice 30 min after a 1 g/kg glucose intraperitoneal injection and showed a relative increase in serum insulin levels (Fig. 2C). Glycogen synthesis in the liver of these mice was also relatively increased after an intraperitoneal injection of 1 g/kg glucose (Fig. 2D). However, due to the small sample size, the data does not have statistical significance (the data is not shown). This suggests that Sema4D $-/-$ mice may have some glycemic lowering

function through the increased expression of GLUT2 in liver and pancreatic β -cells.

Increased expression of GLUT2 in Sema4D $-/-$ mice does not cause differences in glucose tolerance in the normoglycemic state

The IPGTT assay in Sema4D $-/-$ mice showed no significant difference in glucose tolerance between the Sema4D $-/-$ and Sema4D $+/+$ mice during normoglycemia (Fig. 3A). There was also no statistical difference when the mice were compared when grouped according to sex (Fig. 3B, C), with no statistical difference in their body weight. This suggests that GLUT2 in Sema4D $-/-$ mice does not have a significant hypoglycemic effect under normoglycemic conditions even when its levels are elevated. This is due to GLUT2 being a membrane protein involved in passive glucose transport with its dynamics depending on the difference in glucose concentration gradients between the inside and outside of the cell membrane. No significant differences were observed in the insulin tolerance assay (Fig. 3D), and there were no significant differences in body weight. Even when the mice were grouped by sex, there was no significant difference in insulin tolerance during the normoglycemic state. The insulin sensitivity of Sema4D $-/-$ male mice

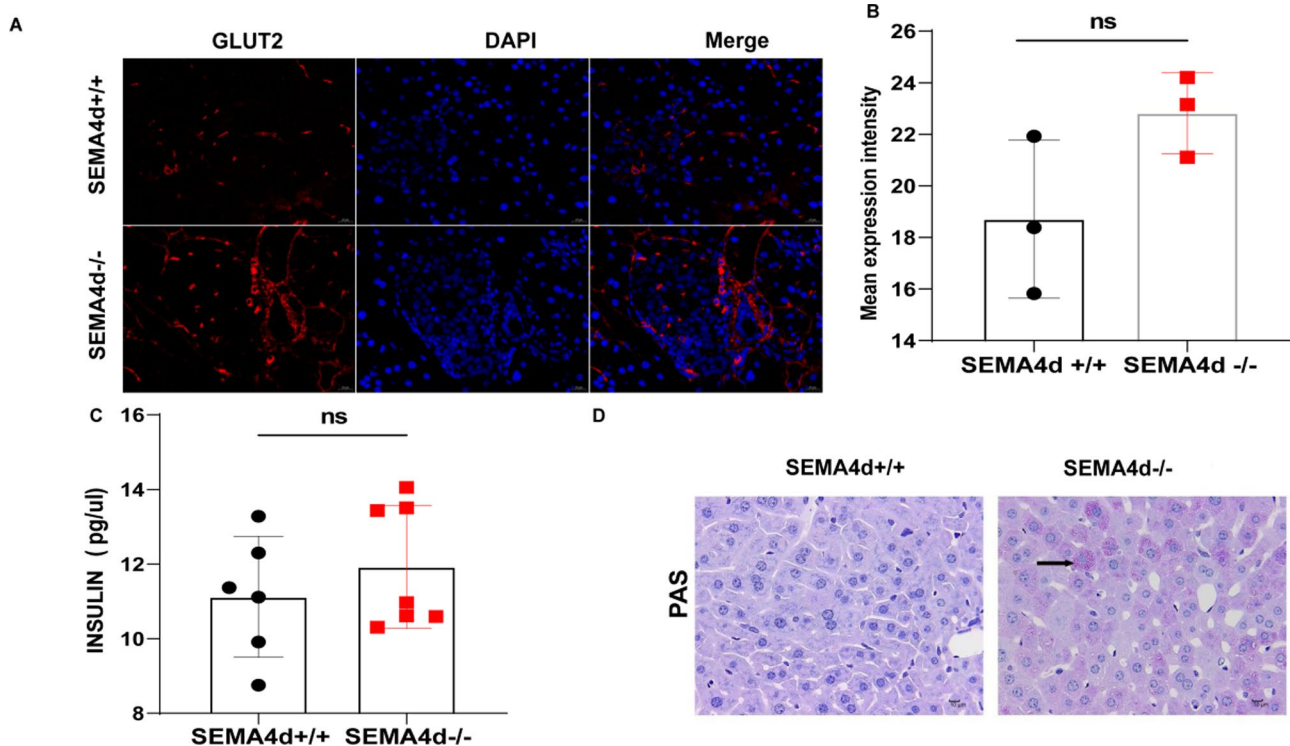


Fig. 2 Glucose-stimulated insulin secretion may be increased in Sema4D $-/-$ mice. Immunofluorescence comparison of GLUT2 expression in pancreatic cells of two groups of mice (A). The DAPI-stained nuclei are blue and GLUT2 positive expression is red. The comparison of fluorescence intensity is shown as mean \pm SD (B). The insulin content in the serum of the two groups of mice after 30 min of glucose stimulation was measured by ELISA, and the results expressed as mean \pm SD (C). The difference in liver glycogen expression between the two groups of mice after 30 min of glucose stimulation was compared by PAS staining (D). The magnifications are 10 \times and 40 \times

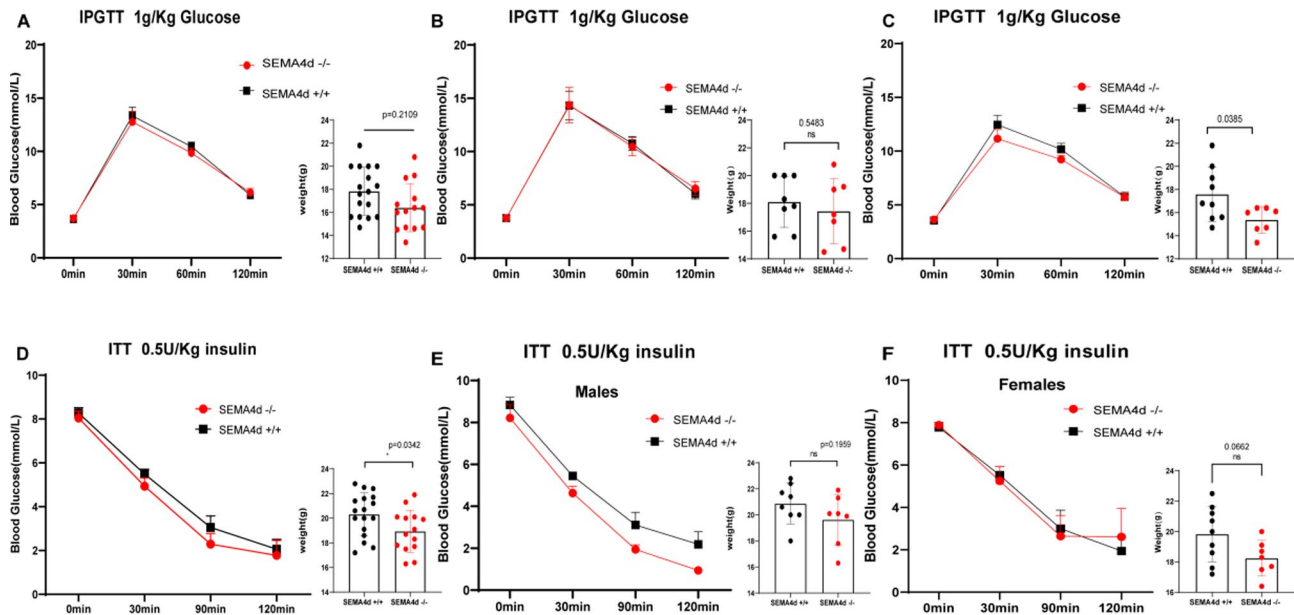


Fig. 3 There were no differences in the glucose and insulin tolerance tests between the *Sema4D*^{-/-} mice and wild-type mice. The glucose tolerance test was performed using 2 g/kg of glucose after 12–16 h of fasting without water in both groups of mice. KO group ($n = 14$) and WT group ($n = 17$) (A). The differences in glucose tolerance test data and body weight between the two groups were compared by gender grouping. Male KO group ($n = 7$) and male WT group ($n = 8$) (B). Female KO group ($n = 7$) and female WT group ($n = 9$) (C). The insulin tolerance test was performed in both groups of mice using 1 U/kg insulin after 4–6 h of fasting without water (D). Differences in the insulin tolerance test data and body weight between the two groups were compared by gender grouping. Male KO group ($n = 7$) and male WT group ($n = 8$) (E). Female KO group ($n = 7$), female WT group ($n = 9$) (F). The results are expressed as mean \pm SD

appeared to be stronger than that of wild-type mice (Fig. 3E). We observed that the insulin tolerance data of *Sema4D*^{-/-} female mice and wild-type mice almost overlapped (Fig. 3F). There may be a mechanism that can raise blood glucose to counteract the hypoglycemic effect to avoid hypoglycemia from occurring. We observed that the body weight of *Sema4D*^{-/-} mice was not statistically different from that of wild-type mice. But the growth and development of the *Sema4D*^{-/-} mice appeared to be slower than that of wild-type mice in the same litter of the same age (data not shown). This suggested that *Sema4D* may have a role in the growth and development rate of mice.

***Sema4D*^{-/-} male mice have greater glucose tolerance in the hyperglycemic state**

After an intraperitoneal injection of 100 mg/kg of STZ, random changes in blood glucose levels were observed at 10:00 am daily after the injection. The response in *Sema4D*^{-/-} mice did not differ significantly from that observed in wild-type mice, with blood glucose increasing almost simultaneously and to approximate similar levels (Fig. 4A). And there was no significant difference in the change of body weight between the two groups of mice (Fig. 4B). One week after the STZ injection, in STZ-induced insulin-deficient diabetes, the blood glucose levels of the mice increased to a more stable level, with an intraperitoneal glucose tolerance test (IPGTT, 1 g/kg)

showing no statistical difference between the *Sema4D*^{-/-} and wild-type mice (Fig. 4C), and no difference in body weight (data not shown). However, comparison of the sex groups showed that *Sema4D*^{-/-} male mice appeared to utilize glucose more rapidly than the wild-type mice (Fig. 4D). The *Sema4D*^{-/-} female mice had an opposite response to that of males, by appearing to exhibit a slower rate of glucose regulation (Fig. 4E). When an intraperitoneal insulin tolerance test (ITT, 0.5 U/kg) was performed two weeks after the STZ injection at randomized glucose stabilization, no statistical differences in ITT or body weight were observed (data not shown). There was also no statistical difference when the male and female mice were compared separately (Fig. 4F). Although the *Sema4D*^{-/-} male mice appeared to be more sensitive to insulin (Fig. 4G), whereas the *Sema4D*^{-/-} female mice did not show any difference in insulin sensitivity from that measured in wild-type mice (Fig. 4H). After STZ injection, knockout mice of different sexes showed opposite glucose tolerance, with *Sema4D*^{-/-} males having lower fasting glucose levels than wild-type males, while the opposite effect was observed in females.

Increased expression of monosaccharide transporter MUP occurs in the liver cytoplasm of *Sema4D*^{-/-} mice

Heat map clustering analysis of genes with statistically different transcript expression showed that expression of the MUP family was upregulated, while the expression

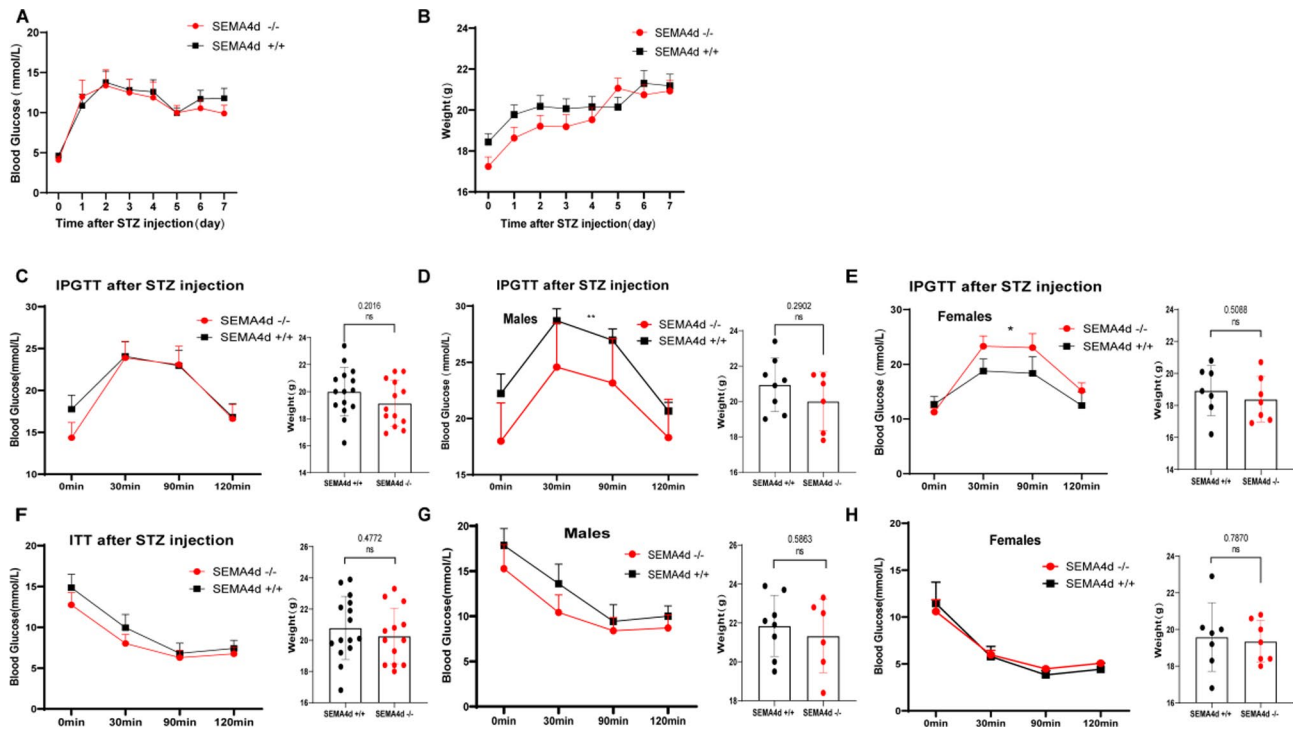


Fig. 4 The glucose tolerance of Sema4D^{-/-} male mice was significantly better than that of wild-type male mice. The two groups of mice were observed continuously for changes in random blood glucose and body weight at 10:00 am after treatment with a single intraperitoneal injection of 100 mg/kg of STZ in the KO group ($n=13$) and WT group ($n=15$) (A). After the random blood glucose became more stable, the mice in both groups were fasted without drinking for 8–12 h and a glucose tolerance test was then performed using 1 g/kg of glucose (B). The comparison of the glucose tolerance test data and body weight difference was performed by gender grouping, male KO group ($n=6$) and male WT group ($n=8$) (C), female KO group ($n=7$), and female WT group ($n=7$) (D). The mice in both groups were fasted without drinking for 4–6 h and an insulin tolerance test was performed using 0.5 U/kg of insulin (E). Comparison of the insulin tolerance test data and difference in body weight was performed by gender grouping (F) (G). All the experimental data were expressed as mean \pm SD

of heavy and light chain antibody families were mostly downregulated (Fig. 5A). According to GO annotation, the MUP family is an important glucose transporter in the cytoplasm positively regulated by glucose-stimulated insulin release. It is also involved in positive regulation of glycogen synthesis and glucose input and regulation of cellular responses to glucose, in conjunction to playing an important role in the regulation of glucose homeostasis. Real-time fluorescence quantitative nucleic acid amplification also verified the corresponding mRNAs with up-regulated expression in the heat map (Fig. 5B). In the KEGG clustering analysis, endocrine and digestive pathways were found to be upregulated, with increased nucleotide and lipid metabolism (Fig. 5C). A bubble map of the top 30 differentially expressed GO enrichment analysis showed a decrease in B cell-mediated immune responses involving antibodies (Fig. 5D), while a bubble map of the top 30 KEGG enrichment analysis pathways showed an increase in nucleotide synthesis pathways (Fig. 5E). The increase in MUP, which plays a role in the maintenance of glucose homeostasis, suggests that in Sema4D^{-/-} mice a hypoglycemic effect may be caused by increasing hepatic MUP expression in combination with increased GLUT2

protein on the cell membrane surface, thereby increasing glucose transport and utilization.

STZ-induced cell apoptosis was not enhanced by increased GLUT2 expression in Sema4D^{-/-} male mice

STZ caused apoptosis through DNA alkylation by entering the cells via GLUT2. Although islet β -cell membrane GLUT2 expression was increased in the Sema4D^{-/-} mice. However, it is possible that 100 mg/kg of STZ did not exceed the transport capacity of GLUT2 protein in the cell membrane of wild-type mice. Accordingly, no significant difference was seen in the damage to pancreatic cells caused by STZ, and despite increased expression of transport protein in Sema4D^{-/-} mice, insulin expression was still observed (Fig. 6A). There was also no statistical difference between the two groups in the comparison of mean fluorescence expression of insulin (Fig. 6B) and glucagon (Fig. 6C). Hepatocytes were seen to have different degrees of vacuolar degeneration, with the cytoplasm of degenerated cells containing more vacuoles of different sizes, and the nucleus hanging in the center or on one side. In addition, some hepatocytes were swollen with a small number of localized hepatocytes displaying

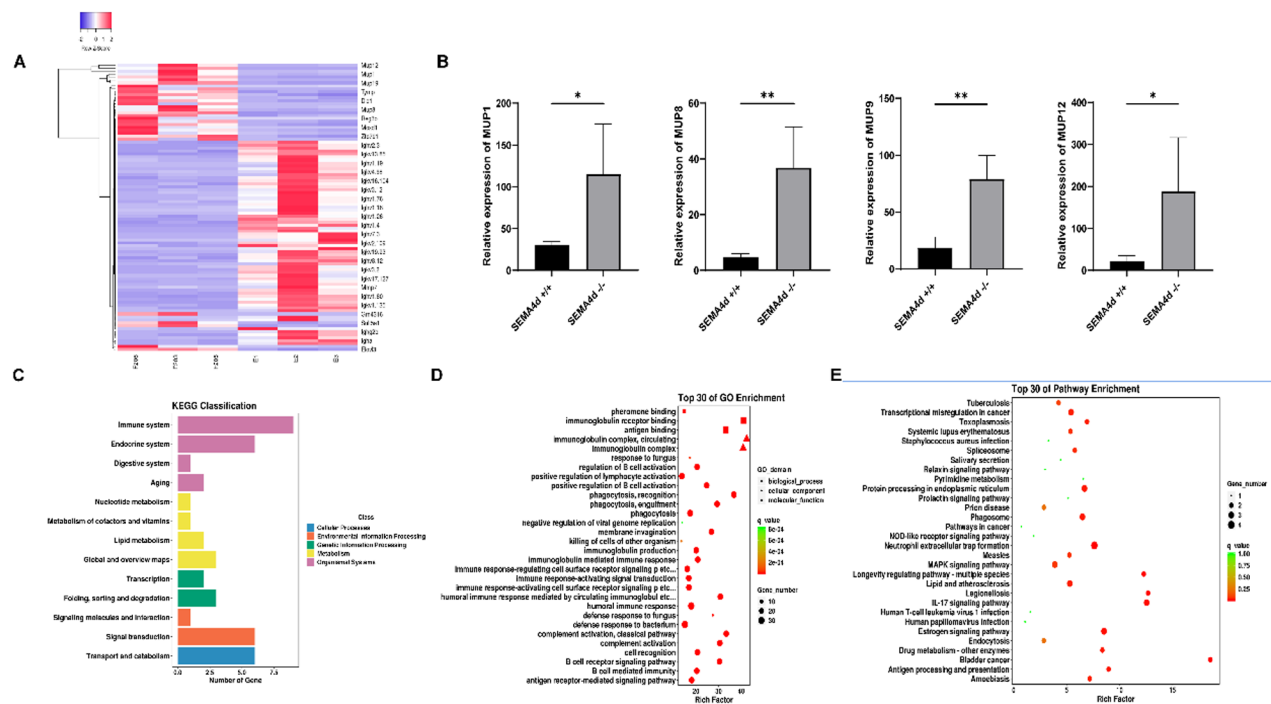


Fig. 5 MUP expression was increased significantly in Sema4D^{-/-} mice. A heat map was drawn from differentially expressed genes, with each row characterizing one gene and each table characterizing one sample (A). RT-PCR verified the expression of MUP mRNA, with the data expressed as mean \pm SD (B). Functional distribution map of differential gene-related pathways based on the KEGG database (C). The GO enrichment results of differential genes are shown as bubble plots (D). The KEGG enrichment results of the differential genes are shown as bubble plots (E). * $p < 0.05$, ** $p < 0.01$

punctate necrosis, cytoplasmic lysis of necrotic cells, nucleus consolidation, and disintegration. A small number of infiltrating inflammatory cells and neutrophils with lobulated or rod-shaped nuclei were also observed (Fig. 6D). A small number of islet cells were degenerated and necrotic, with the necrotic cells being swollen with a blurred structure, cytoplasmic vacuolization, and cytosolic consolidation or lysis (Fig. 6E). No significant differences in liver inflammation or islet cell destruction were seen between the two groups.

Although hepatic glycogen expression was higher in the STZ-injected mice than in the normoglycemic state, there was no statistical difference between the two groups (Fig. 6F). This suggests that in the hyperglycemic state, both groups passively receive more glucose input and glycogen synthesis to lower blood glucose. There was almost no significant change in glycogen synthesis in muscle compared to that seen normally (Fig. 6G), and there was no statistically significant difference between the two groups. This may be related to the fact that muscle glycogen synthesis is not involved in the regulation of blood glucose, but only to energy expenditure of the muscle itself, and therefore muscle glycogen expression remained lower. The expression of GLUT2 and GLUT2 mRNA on the cell membrane surface decreased after the STZ injection, a change which has been reported in previous literature. However, the Sema4D^{-/-} mice still

retained GLUT2 expression to a greater extent than that observed in the wild-type mice (Fig. 6H), with this difference being significantly different. This may be the basis of the vector that Sema4D^{-/-} male mice can utilize blood glucose faster than wild-type mice.

Sema4D^{-/-} male mice have attenuated insulin resistance in the early hyperglycemic state

After the STZ injection, the mice showed reduced levels of serum insulin compared to that measured before the injection (data not shown). The chronological appearance of insulin secretion in glucose-stimulated mice appeared normal (Fig. 7A). However, after grouping by sex, the Sema4D^{+/+} male mice showed hyperinsulinemia with early type 2 diabetes insulin resistance and lost the normal chronological appearance of insulin secretion observed in glucose-stimulated mice, whereas the Sema4D^{-/-} male mice still showed normal glucose-stimulated insulin secretion (Fig. 7B). In contrast, female mice showed exactly the opposite response (Fig. 7C). The levels of serum C-peptide in the mice were more consistent with insulin secretion, with more C-peptide secretion in Sema4D^{-/-} mice (Fig. 7D) and significantly more in male Sema4D^{-/-} mice than in wild-type mice (Fig. 7E). This indicated that insulin secretion was greater and normal after glucose-stimulation, while the opposite result was observed in the female Sema4D^{-/-} mice (Fig. 7F).

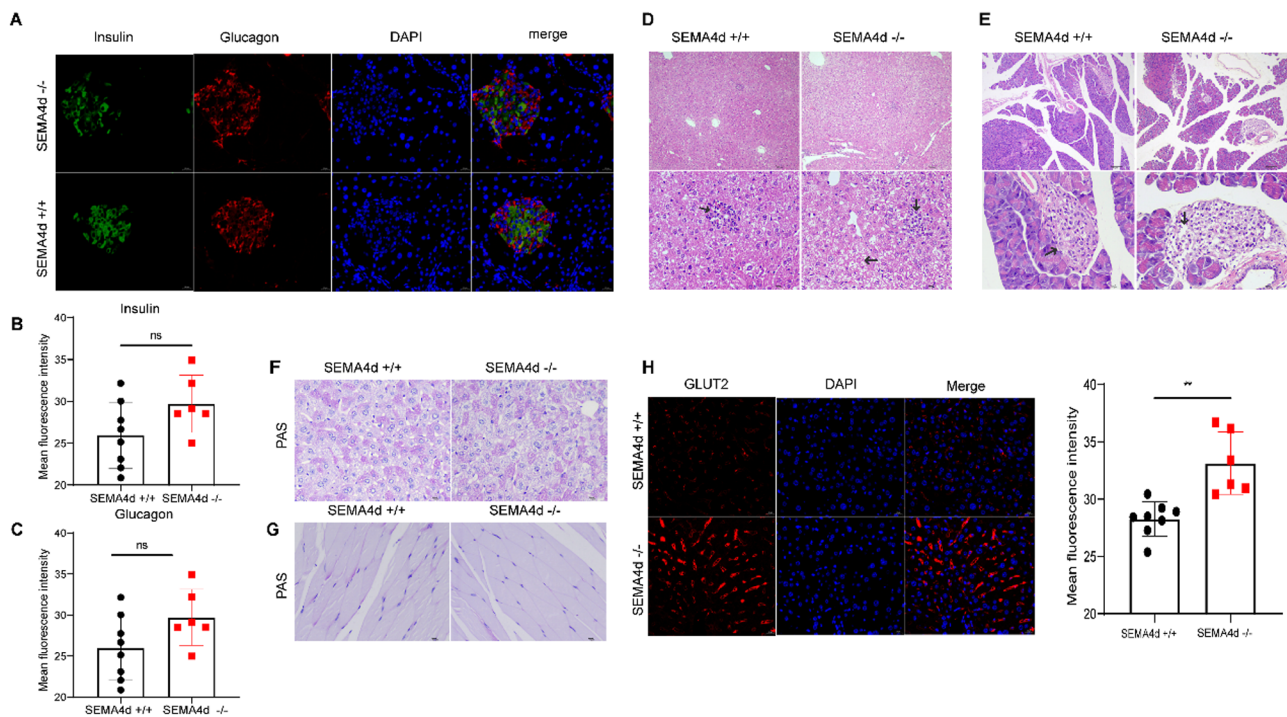


Fig. 6 There was no significant difference in islet and liver destruction in *Sema4D*^{-/-} male mice by STZ. Immunofluorescence detection of differences in insulin and glucagon expression in male mice islet cells after STZ treatment at a dose of 100 mg/kg (A). DAPI stained cell nuclei in blue, glucagon positive expression in red, and insulin positive expression in green. KO group ($n=6$) (B), WT group ($n=8$) (C). Comparison of HE staining. Cellular inflammation and destruction in liver (D) and pancreas (E) of mice in both groups after STZ treatment. The black arrows indicate various pathological injuries to the tissues; these include punctate necrosis of cells and infiltration of inflammatory cells. PAS staining was performed to compare the differences in liver glycogen (F) and muscle glycogen (G) synthesis between the two groups. The differences in hepatic GLUT2 expression between the two groups of male mice after STZ treatment were analyzed by immunofluorescence (H), with DAPI-stained nuclei in blue and GLUT2-positive expression in red. The mean fluorescence intensity expressions were obtained by Image J and all were expressed as mean \pm SD. The magnifications are 10x and 40x. * $p < 0.05$, ** $p < 0.01$

There was little difference in serum glycated albumin levels in the mice (Fig. 7G), which was consistent with the random blood glucose results measured earlier.

Sema4D^{-/-} male mice have enhanced metabolism of the pentose phosphate pathway

The expression of metabolites in the *Sema4D*^{-/-} and *Sema4D*^{+/+} groups could be better grouped as seen by orthogonal-partial least squares discriminant analysis OPLS-DA reduced dimensional analysis (Fig. 8A). The heat map showed an increase relative to the WT group with an increase in metabolites such as N-acetylleucine, leukotriene C4, D-ribulose 5-phosphate, NADP, GMP, and a decrease in docosapentaenoic acid (Fig. 8B). Among these metabolites, D-ribulose 5-phosphate is involved in the metabolism of the pentose phosphate pathway, which provides substrate feedstock for purine anabolism by consuming glucose to produce ribose. The network plot showed enhanced biometabolism of the pentose phosphate pathway and purine synthesis pathway, and reduced metabolism of the citric acid cycle pathway (Fig. 8C). The z-score plots showed a difference in expression of differential metabolites between the

two groups (Fig. 8D). The horizontal coordinate is the relative amount of metabolites in the group after z-score conversion, with more metabolites on the right side indicating more metabolites in the group. The bubble map showed an enhanced vitamin B6 metabolic pathway and a diminished antibody Fc segment-mediated immune response, findings which were consistent with the transcriptome sequencing results (Fig. 8E). The enhancement of the pentose phosphate pathway associated with glucose metabolism suggests that *Sema4D*^{-/-} mice may exert hypoglycemic effects by increasing ribose synthesis through a glucose metabolic bypass. The downstream purine metabolic pathway was also seen to be enhanced. Two pathways directly involved in the metabolism of sugar-water compounds were enriched, namely the inter-conversion of pentose and glucuronide, and the pentose phosphate pathway (Fig. 8F). This suggests that *Sema4D*^{-/-} mice may lower blood glucose levels through catabolism of glucose. In conclusion, *Sema4D*^{-/-} male mice exert glucose-lowering effects through increased expression of GLUT2. Increased glucose catabolism through the pentose phosphate pathway, purine anabolism, and insulin secretion stimulated by glucose (Fig. 8G).

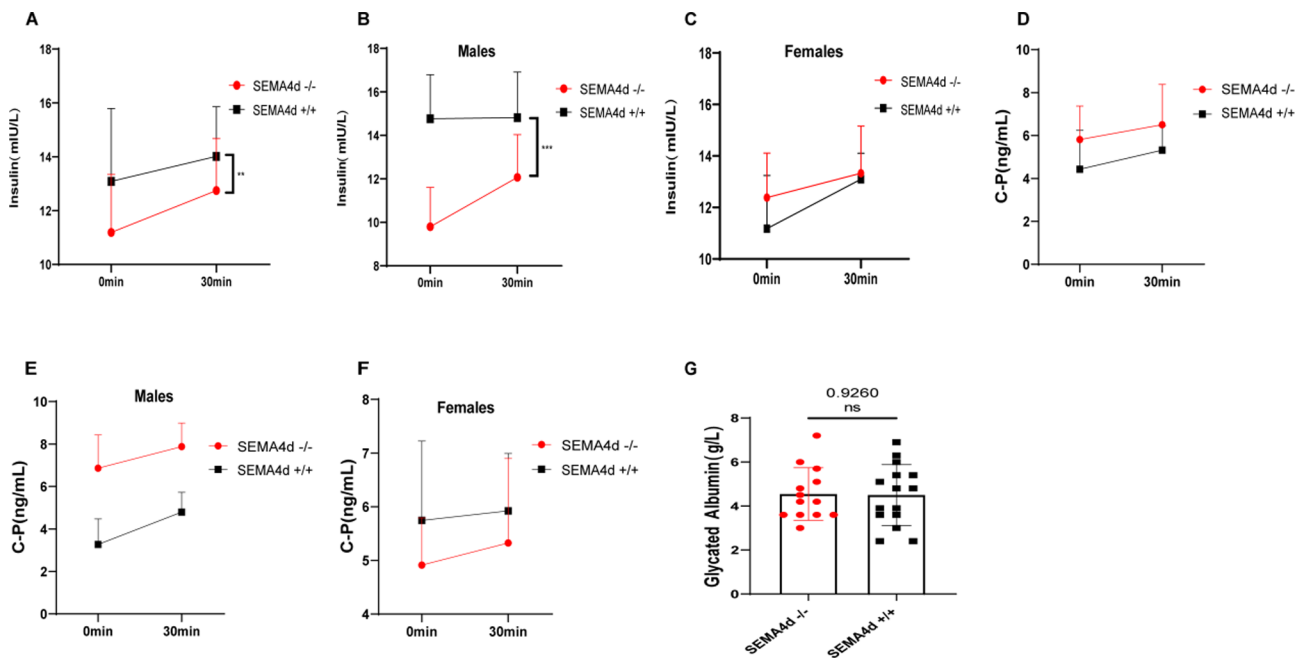


Fig. 7 *Sema4D*^{-/-} male mice did not exhibit insulin resistance during the early hyperglycemic state. Serum insulin levels were measured in both groups of mice following an intraperitoneal injection of 1 g/kg of glucose after 4–6 h of fasting, 0 min before and 30 min after injection. KO group ($n = 13$), WT group ($n = 15$) (A), comparison by sex grouping, male KO group ($n = 6$), male WT group ($n = 8$) (B), female KO group ($n = 7$), and female WT group ($n = 7$) (C). The levels of C-peptide in the serum at the same time points were also measured (D) and compared according to gender grouping (E, F). Serum glycated albumin levels were measured in both groups of mice (G). All the data are expressed as mean \pm SD

Discussion

GLUT2 is expressed specifically in mice liver and pancreatic β -cells and is the most important glucose transporter protein in mice, with knockdown of SLC2A2, the gene that mediates GLUT2, resulting in non-viable mice. Neonatal deficiency of GLUT2 is known as Fanconi syndrome, which manifests mainly as an overall dysfunction of the proximal tubule, leading to excessive urinary excretion of amino acids, glucose, phosphate, bicarbonate, uric acid, and other solutes reabsorbed by the renal unit segment [9]. These changes may lead to transient diabetes mellitus but resolve spontaneously with age in most individuals, probably due to GLUT1 and GLUT3. These responses also suggest that GLUT2 has an important role in the early human pancreas for the release of insulin in response to glucose stimulation, although this role can be superseded by other glucose transporter proteins [9]. GLUT2-deficient mice do not receive compensatory regulation by GLUT1 as well as GLUT3, although glucose can still be transported at a slower rate through the remaining glucose transporter proteomes despite the insulin-producing effect being significantly impaired [15]. An abundance of GLUT2 protein is comparable in human and rat liver, with the transport function performed by GLUT2 in rat pancreatic β -cells appearing to be replaced by GLUT1 and/or GLUT3 in human pancreatic β -cells [16]. Therefore, GLUT2 (SLC2A2) may not be the major glucose transporter protein in human

pancreatic β -cells. However, a variant rs8192675 in the SLC2A2 gene (C allele) was shown recently to be associated with an improved glucose response to metformin monotherapy in the first year following diagnosis of type 2 diabetes [10]. Patients with GLUT2 gene defects have reduced glycogen synthesis due to diminished glucose substrate transport. The recent discovery of a method that can be used to study diabetes caused by pure mutations in the human SLC2A2 gene [17] will help us to explore more deeply the specific role of GLUT2 in human glucose metabolism.

There is evidence that glucose transporter-2 (GLUT2) promoter-mediated production of transgenic insulin reduces hyperglycemia in diabetic mice [18]. Metformin treatment increased the GLUT2 transporter, which may be an alternative pathway to lower hypoglycemic levels in the diabetic state [10]. This activation of PXR induces hyperglycemia by impairing hepatic glucose metabolism through inhibition of the hepatocyte nuclear factor 4- α (HNF4 α) glucose transporter 2 (GLUT2) pathway. The PXR agonists, atorvastatin and rifampin significantly downregulate GLUT2 and HNF4 α expression and impair glucose uptake and utilization in HepG2 cells [19]. Downregulation of GLUT2 expression affects the dynamic translocation of GLUT2 to the rptc brush border membrane and decreases glucose reabsorption, thereby exacerbating the development of diabetic nephropathy. Elevated levels of glucose and/or its

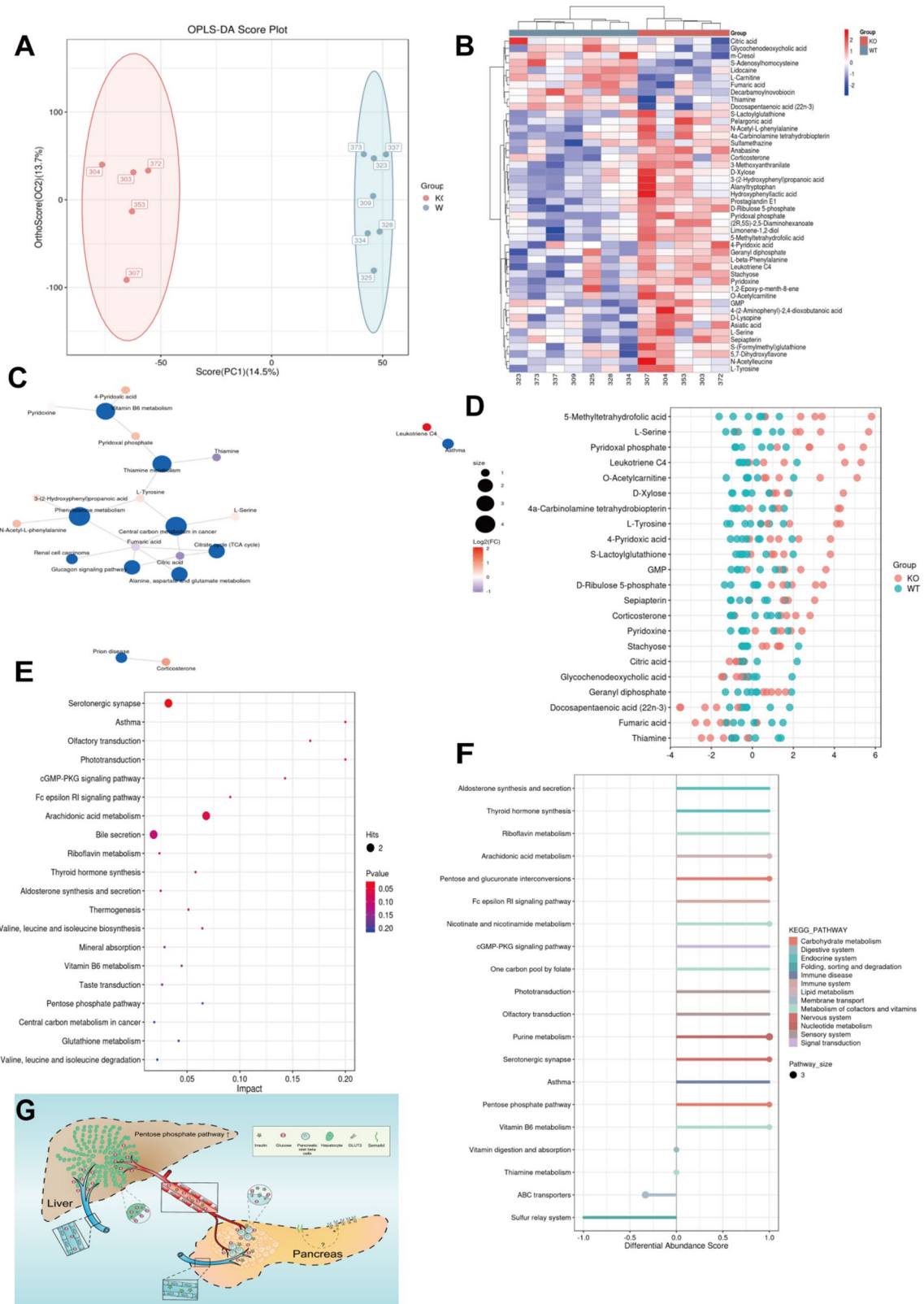


Fig. 8 (See legend on next page.)

(See figure on previous page.)

Fig. 8 Enhanced metabolism of the pentose phosphate pathway in *Sema4D*^{-/-} male mice. Comparison of differences in metabolite expression between the two groups as seen by orthogonal-partial least squares discriminant analysis of OPLS-DA (**A**). Hierarchical clustering heat map of differential metabolites (**B**), where the magnitude of the relative content is shown by the difference in color, with the redder the color showing higher expression, while the bluer the color showing lower expression. The columns represent samples and the rows represent metabolite names. Network diagram of differential metabolites (**C**), with blue dots indicating pathways and the other dots indicating metabolites. The size of the pathway points indicates a larger number of metabolites connected to it, while the metabolite points indicate the size of log₂ (FC) values according to gradient color, with multiple groups comparing no metabolite log₂ (FC) information. The relative size of the content in the graph is indicated by the color difference, with the redder color showing higher expression and the bluer color showing lower expression. A z-score plot (**D**). The vertical coordinate shows the name of the metabolite, the color of the dot represents the different groups, the horizontal coordinate is the relative content of the metabolite in the group obtained by z-score conversion, with those more to the right representing more metabolites in the group. Metabolic pathway impact factor bubble diagram (**E**). Each point represents a metabolic pathway, with the horizontal coordinate showing the impact value enriched to different metabolic pathways, and the vertical coordinate showing the enriched pathway. The dots indicate the number of corresponding metabolic molecules in the pathway. The color correlates with the *P* value, with redder color representing smaller *P* values, and bluer color representing larger *P* values. Differential enrichment score plot (**F**). The horizontal coordinate is the DA-score value calculated using the formula DA-score = (number of upregulated substances - number of downregulated substances) / total number of differential substances on that pathway. The vertical coordinate is the metabolic pathway, with the size of the top point of the bar indicating the number of differential metabolites enriched in that pathway. Schematic representation of the increased involvement of GLUT2 in the regulation of glucose metabolism after knockdown of *Sema4D*, with the graphic drawn by Adobe Illustrator (**G**)

metabolites in renal tubular cells may be necessary for the development of tubulopathy and diabetic-like glomerular disease associated with GLUT2 deficiency [20]. Taken together, these findings suggest that GLUT2 has an important role in the hypoglycemic effect and alleviation of diabetic complications. However, it has also been reported that during diabetic hyperglycemia, GLUT2-mediated enhancement of glucose transport through the proximal tubule brush border microvilli (BBM) is associated closely with an increase in PKC- β I. Therefore, alterations in GLUT2 and PKC- β I protein levels in the BBM may be important in the pathogenesis of diabetic kidney injury [21].

We used a single intraperitoneal injection of STZ (100 mg/kg) to establish a mouse model of hyperglycemia. The degree of damage to pancreatic β -cells and hepatocytes caused by STZ correlated positively with GLUT2 expression, with STZ destroying GLUT2-positive cells mainly by promoting the release of inflammatory factors. It has been shown that STZ induces diabetes through β -cell apoptosis after being transported by GLUT2 and increases expression of inflammatory genes, with the release of inflammatory factors promoting destruction of pancreatic β -cells thereby leading to insulin-deficient blood glucose [22]. mPGES-2 wild-type (WT) and knockout (KO) mice with type 1 diabetes induced by a single intraperitoneal dose of 120 mg/kg of STZ, resulted in the mPGES-2KO mice having increased GLUT2 expression with STZ treatment leading to liver inflammation [23]. However, this phenomenon was not observed in our experimental model, which may be due to the different dosage of STZ or to differences in immune responsiveness between these two knockout mice models. It has been reported that bcr-mediated signaling is enhanced in CD72-deficient cells but reduced in *Sema4D*-deficient cells [24]. The *Sema4D*^{-/-} male mice in our study had an attenuated antibody-mediated immune response, a result which was consistent with the transcriptome sequencing

and metabolomic analysis in our study. Reduced GLUT2 expression attenuates STZ damage to pancreatic β -cells and reduces insulin release induced by glucose stimulation. However, increased GLUT2 expression does not necessarily increase the destruction of pancreatic β -cells caused by STZ. Liver and pancreatic β -cells of mice mainly express GLUT2 transporters. A dose of 100 mg/kg of STZ may not exceed the GLUT2 transport capacity of wild-type mice and therefore even an increase in the number of transporters may not exacerbate the damage to GLUT2-positive cells caused by STZ.

Despite increased GLUT2 expression in *Sema4D*^{-/-} mice hepatocytes, the mice did not show a stronger hypoglycemic effect than wild-type mice during normoglycemic states, with glucose uptake not being dependent on the number and activity of glucose transporters, but rather on blood glucose or glucose analogue blood concentrations [25]. GLUT2 is a high glucose receptor, although it has also been reported to have a uniquely high *K_m* for glucose (~17 mM) that allows rapid glucose homeostasis between the extracellular space and the cytoplasm at all physiological or diabetes-related glucose levels [26].

Although hyperglycemia was less pronounced, diastolic dysfunction was more pronounced in STZ-induced diabetic female mice [27]. Reduced circulating estradiol levels and imbalance in renal estrogen receptor expression accelerate the progression of diabetic nephropathy [28]. Insulin sensitivity and susceptibility to diabetes are indeed associated with sex differences [29]. However, it has also been reported that establishing equivalent diabetes in male and female *Nos3*-deficient mice results in a comparable onset of diabetic kidney injury [30].

However, the specific mechanism of the increase in GLUT2 transporters mediated in the *sema4D*^{-/-} male mouse model for glucose regulation remains to be further investigated. Currently, we have observed a significant slowdown in cell growth compared to the negative

control group by lentiviral transfection of mouse hepatocytes and gastric cancer cell lines. We now hypothesize that perhaps the silencing of SEMA4d expression affects cell growth and that the cells compensate by increasing GLUT2 to obtain more energy material in order to avoid growth restriction.

Abbreviations

Sema4D/CD100	Semaphorin 4D or cluster of differentiation 100
GLUT2	The glucose transporter 2
T2D	Type 2 diabetes mellitus
STZ	Streptozotocin
HE stains	Hematoxylin stains

Supplementary Information

The online version contains supplementary material available at <https://doi.org/10.1186/s12967-024-05694-7>.

Supplementary Material 1

Supplementary Material 2

Acknowledgements

This work was supported by the Department of Science and Technology of Sichuan Province Grant numbers (2021YFS0375, 2022YFS0157), the National Natural Science Foundation of China (No. 81172832, 81771723). The authors would like to express their gratitude to EditSprings (<https://www.editsprings.cn>) for the expert linguistic services provided.

Author contributions

Y.Z. and X.J. designed the study, analyzed the data and with Y.Z. and G.J. wrote the manuscript; Y.Z., H.H., X.J., and D.W. completed the experimental operation to record the experimental data; Y.C. provided pre-experimental data. Y.Z., X.J., and G.Z. were the guarantors of this work and, as such, had full access to all the data in the study and take responsibility for the integrity of the data and the accuracy of the data analysis.

Data availability

The data that support the findings of this study are available from the corresponding author upon reasonable request.

Declarations

Conflict of interest

No potential conflict of interest relevant to this article are reported.

Received: 4 July 2024 / Accepted: 18 September 2024

Published online: 27 September 2024

References

1. Wu T, Zhang S, Xu J, Zhang Y, Sun T, Shao Y, Wang J, Tang W, Chen F, Han X. HRD1, an important player in pancreatic β -Cell failure and therapeutic target for type 2 Diabetic mouse. *Diabetes*. 2020;69(5):940–53. <https://doi.org/10.2337/db19-1060>.
2. Li S, Vandvik P, O., Lytvyn L, Guyatt G, H., Palmer S, C., Rodriguez-Gutierrez R, Foroutan F, Agoritsas T, Siemieniuk R, Walsh M, Frere L, Tunnicliffe D, J., Nagler E, V., Manja V, Åsvold B, O., Jha V, Vermandere M, Gariani K, Zhao Q, Ren Y, ... Mustafa R. A. (2021). SGLT-2 inhibitors or GLP-1 receptor agonists for adults with type 2 diabetes: a clinical practice guideline. *BMJ (Clinical research ed.)*, 373, n1091. <https://doi.org/10.1136/bmj.n1091>.
3. Thorens B. GLUT2, glucose sensing and glucose homeostasis. *Diabetologia*. 2015;58(2):221–32. <https://doi.org/10.1007/s00125-014-3451-1>.
4. Liu R, Liu C, He X, Sun P, Zhang B, Yang H, Shi W, Ruan Q. MicroRNA-21 promotes pancreatic β cell function through modulating glucose uptake. *Nat Commun*. 2022;13(1):3545. <https://doi.org/10.1038/s41467-022-31317-0>.
5. Ding L, Han L, Dube J, Billadeau DD. WASH regulates glucose homeostasis by facilitating GLUT2 receptor recycling in pancreatic β -Cells. *Diabetes*. 2019;68(2):377–86. <https://doi.org/10.2337/db18-0189>.
6. Wang T, Jiang H, Cao S, Chen Q, Cui M, Wang Z, Li D, Zhou J, Wang T, Qiu F, Kang N. Baicalin and its metabolites suppresses gluconeogenesis through activation of AMPK or AKT in insulin resistant HepG-2 cells. *Eur J Med Chem*. 2017;141:92–100. <https://doi.org/10.1016/j.ejmech.2017.09.049>.
7. Berry GT, Baynes JW, Wells-Knecht KJ, Szverglod BS, Santer R. Elements of diabetic nephropathy in a patient with GLUT 2 deficiency. *Mol Genet Metab*. 2005;86(4):473–7. <https://doi.org/10.1016/j.ymgme.2005.09.010>.
8. Laukkanen O, Lindström J, Eriksson J, Valle TT, Hämäläinen H, Ilanne-Parikka P, Keinänen-Kiukkaanniemi S, Tuomilehto J, Uusitupa M, Laakso M, Finnish Diabetes Prevention Study. Polymorphisms in the SLC2A2 (GLUT2) gene are associated with the conversion from impaired glucose tolerance to type 2 diabetes: the Finnish diabetes Prevention Study. *Diabetes*. 2005;54(7):2256–60. <https://doi.org/10.2337/diabetes.54.7.2256>.
9. Liang X, Giacomini KM. Transporters involved in Metformin Pharmacokinetics and Treatment Response. *J Pharm Sci*. 2017;106(9):2245–50. <https://doi.org/10.1016/j.xphs.2017.04.078>.
10. Sun Q, Zhou H, Binmadi NO, Basile JR. Hypoxia-inducible factor-1-mediated regulation of semaphorin 4D affects tumor growth and vascularity. *J Biol Chem*. 2009;284(46):32066–74. <https://doi.org/10.1074/jbc.M109.057166>.
11. Wang F, Liu B, Yu Z, Wang T, Song Y, Zhuang R, Wu Y, Su Y, Guo S. Effects of CD100 promote wound healing in diabetic mouse. *J Mol Histol*. 2018;49(3):277–87. <https://doi.org/10.1007/s10735-018-9767-2>.
12. Wu JH, Li YN, Chen AQ, Hong CD, Zhang CL, Wang HL, Zhou YF, Li PC, Wang Y, Mao L, Xia YP, He QW, Jin HJ, Yue ZY, Hu B. Inhibition of Sema4D/PlexinB1 signaling alleviates vascular dysfunction in diabetic retinopathy. *EMBO Mol Med*. 2020;12(2):e10154. <https://doi.org/10.15252/emmm.201810154>.
13. Guillam MT, Dupraz P, Thorens B. Glucose uptake, utilization, and signaling in GLUT2-null islets. *Diabetes*. 2000;49(9):1485–91. <https://doi.org/10.2337/diabetes.49.9.1485>.
14. Liu C, Zhang C, He T, Sun L, Wang Q, Han S, Wang W, Kong J, Yuan F, Huang J. Study on potential toxic material base and mechanisms of hepatotoxicity induced by *Dysosma Versipellis* based on toxicological evidence chain (TEC) concept. *Ecotoxicol Environ Saf*. 2020;190:110073. <https://doi.org/10.1016/j.ecoenv.2019.110073>.
15. Enogieru OJ, Ung P, Yee SW, Schlessinger A, Giacomini KM. Functional and structural analysis of rare SLC2A2 variants associated with Fanconi-Bickel syndrome and metabolic traits. *Hum Mutat*. 2019;40(7):983–95. <https://doi.org/10.1002/humu.23758>.
16. Shi YL, Zhang YP, Luo H, Xu F, Gao JM, Shi JS, Gong QH. Trilobatin, a Natural Food Additive, exerts anti-type 2 diabetes effect mediated by Nrf2/ARE and IRS-1/GLUT2 signaling pathways. *Front Pharmacol*. 2022;13:828473. <https://doi.org/10.3389/fphar.2022.828473>.
17. Hassani-Nezhad-Gashti F, Rysä J, Kummu O, Nääpänkangas J, Buler M, Karpale M, Hukkanen J, Hakkola J. Activation of nuclear receptor PXR impairs glucose tolerance and dysregulates GLUT2 expression and subcellular localization in liver. *Biochem Pharmacol*. 2018;148:253–64. <https://doi.org/10.1016/j.bcp.2018.01.001>.
18. Hinden L, Udi S, Drori A, Gammal A, Nemirovski A, Hadar R, Baraghithy S, Permyakova A, Geron M, Cohen M, Tsytkin-Kirschenschweig S, Riahi Y, Leibowitz G, Nahmias Y, Priel A, Tam J. Modulation of renal GLUT2 by the Cannabinoid-1 receptor: implications for the treatment of Diabetic Nephropathy. *J Am Soc Nephrol*: JASN. 2018;29(2):434–48. <https://doi.org/10.1681/ASN.2017040371>.
19. Goestemeyer AK, Marks J, Srail SK, Debnam ES, Unwin RJ. GLUT2 protein at the rat proximal tubule brush border membrane correlates with protein kinase C (PKC)-beta and plasma glucose concentration. *Diabetologia*. 2007;50(10):2209–17. <https://doi.org/10.1007/s00125-007-0778-x>.
20. Bellenger J, Bellenger S, Bataille A, Massey KA, Nicolaou A, Rialland M, Tessier C, Kang JX, Narce M. High pancreatic n-3 fatty acids prevent STZ-induced diabetes in fat-1 mouse: inflammatory pathway inhibition. *Diabetes*. 2011;60(4):1090–9. <https://doi.org/10.2337/db10-0901>.
21. Goyal SN, Reddy NM, Patil KR, Nakhate KT, Ojha S, Patil CR, Agrawal YO. Challenges and issues with streptozotocin-induced diabetes - A clinically relevant animal model to understand the diabetes pathogenesis and evaluate therapeutics. *Chemico-Biol Interact*. 2016;244:49–63. <https://doi.org/10.1016/j.cbi.2015.11.032>.

22. Sun Y, Jia Z, Yang G, Kakizoe Y, Liu M, Yang KT, Liu Y, Yang B, Yang T. mPGES-2 deletion remarkably enhances liver injury in streptozotocin-treated mouse via induction of GLUT2. *J Hepatol*. 2014;61(6):1328–36. <https://doi.org/10.1016/j.jhep.2014.07.018>.
23. Xu J, Zhang L, Chou A, Allaby T, Bélanger G, Radziuk J, Jasmin BJ, Miki T, Seino S, Renaud JM. KATP channel-deficient pancreatic beta-cells are streptozotocin resistant because of lower GLUT2 activity. *Am J Physiol Endocrinol Metab*. 2008;294(2):E326–35. <https://doi.org/10.1152/ajpendo.00296.2007>.
24. Uldry M, Ibberson M, Hosokawa M, Thorens B. GLUT2 is a high affinity glucosamine transporter. *FEBS Lett*. 2002;524(1–3):199–203. [https://doi.org/10.1016/s0014-5793\(02\)03058-2](https://doi.org/10.1016/s0014-5793(02)03058-2).
25. Thorens B, Mueckler M. Glucose transporters in the 21st Century. *Am J Physiol Endocrinol Metab*. 2010;298(2):E141–5. <https://doi.org/10.1152/ajpendo.00712.2009>.
26. Chandramouli C, Reichelt ME, Curl CL, Varma U, Bienvenu LA, Koutsifeli P, Raaijmakers A, De Blasio MJ, Qin CX, Jenkins AJ, Ritchie RH, Mellor KM, Delbridge L. Diastolic dysfunction is more apparent in STZ-induced diabetic female mice, despite less pronounced hyperglycemia. *Sci Rep*. 2018;8(1):2346. <https://doi.org/10.1038/s41598-018-20703-8>.
27. Wells CC, Riazi S, Mankhey RW, Bhatti F, Ecelbarger C, Maric C. Diabetic nephropathy is associated with decreased circulating estradiol levels and imbalance in the expression of renal estrogen receptors. *Gend Med*. 2005;2(4):227–37. [https://doi.org/10.1016/s1550-8579\(05\)80052-x](https://doi.org/10.1016/s1550-8579(05)80052-x).
28. Choi JW, Aseer KR, Chaudhari HN, Mukherjee R, Choi M, Yun JW. Gender dimorphism in regulation of plasma proteins in streptozotocin-induced diabetic rats. *Proteomics*. 2013;13(16):2482–94. <https://doi.org/10.1002/pmic.201200529>.
29. Choi M, Choi JW, Chaudhari HN, Aseer KR, Mukherjee R, Yun JW. (2013). Gender-dimorphic regulation of skeletal muscle proteins in streptozotocin-induced diabetic rats. *Cellular physiology and biochemistry: international journal of experimental cellular physiology, biochemistry, and pharmacology*, 31(2–3), 408–20. <https://doi.org/10.1159/000343378>
30. Tian L, Nikolic-Paterson DJ, Tesch GH. Establishing equivalent diabetes in male and female Nos3-deficient mice results in a comparable onset of diabetic kidney injury. *Physiological Rep*. 2019;7(18):e14197. <https://doi.org/10.14814/phy2.14197>.

Publisher's note

Springer Nature remains neutral with regard to jurisdictional claims in published maps and institutional affiliations.